Aeroelastic Response of an Airfoil-Flap System Exposed to Time-Dependent Disturbances

Jae-Hong Shim
Assistant Professor, Department of Control and Measurement Engineering Korea Polytechnic University, Kyungi-do, Korea
Sungsoo Na*
Associate Professor, Corresponding Author, Department of Mechanical Engineering, Korea University, Anam-dong, Sungbuk-ku, Seoul 136-701, Korea
Chan-Hun Chung
Department of Mechanical Engineering, Korea University, Anam-dong, Sungbuk-ku, Seoul 136-701, Korea

Aeroelastic response and control of airfoil-flap system exposed to sonic-boom, blast and gust loads in an incompressible subsonic flowfield are addressed. Analytical analysis and pertinent numerical simulations of the aeroelastic response of 3-DOF airfoil featuring plunging-pitching-flapping coupled motion subjected to gust and explosive pressures in terms of important characteristic parameters specifying configuration envelope are presented. The comparisons of uncontrolled aeroelastic response with controlled one of the wing obtained by feedback control methodology are supplied, which is implemented through the flap torque to suppress the flutter instability and enhance the subcritical aeroelastic response to time-dependent excitations.

Key Words : Aeroelastic Response, Blast Load, Sonic-Boom, Flap, LQG

Nomenclature

A : System matrix for first order differential equation
A_iB_i : Aerodynamic lag state variables
α : Elastic pitch angle
b : Semi-chord
B : Control input matrix
β : Flap angle
c : Nondimensional distance to flap hinge line from the elastic axis
C : Output matrix
d : Nondimensional distance to elastic axis from leading edge
G : Disturbance input matrix
g_h, g_α : Velocity control gains in plunge and pitch, respectively
h : Plunging displacement
I : Identity matrix
I_α, I_β : Inertia in pitch and of the flap
K : Stiffness matrix
K_c : Control gain matrix
K_α, K_β, K_h : Stiffness of pitch, flap and plunge spring
L : Filter gain matrix
L, M : Aerodynamic lift and moment, respectively
M : Mass matrix
S_α, S_β : Static moment of pitch and flap angles
T : Unsteady torque moment of flap spring
u(t) : Control input vector
V_f or V : Flight speed
V_F : Flutter speed
w_G : Gust vertical velocity
w(t) : External disturbance
x, y : Horizontal and vertical coordinates

* Corresponding Author,
E-mail : nass@korea.ac.kr
TEL : +82-2-3290-3370; **FAX** : +82-23-926-9290
Department of Mechanical Engineering, Korea University Anam-dong, Sungbuk-ku, Seoul 136-701, Korea.
(Manuscript **Received** May 10, 2003; **Revised** January 30, 2004)

x_{EA} : Elastic axis position from the mid-chord, positive rearward
Y : Column vector of plunge, pitch and flap displacement
$[\ ]^T$: Transpose of a matrix

1. Introduction

The increasing need for highly flexible, and light weight structural flight vehicles, capable of operating in severe environmental conditions requires to be exposed to more severe environmental conditions than in the past. This requires a great deal of research toward a deeper understanding of the effects of arbitrary time-dependent external excitations, such as blasts, fuel explosions, sonic-booms, and gust loads etc. (Marzocca et al., 2001 ; 2002)

Under such circumstances, even in the condition of flight below the flutter speed, the wing structure will be subjected to large oscillations that can result in its failure by fatigue. Passive methods to overcome the problem include added structural stiffness, mass balancing, trailing edge modification, and speed restrictions. (Yoo, 2001) However, all these attempts to enlarge the operational flight envelope and to enhance the aeroelastic response result in significant weight penalties, or in unavoidable reduction of nominal performances. In this regard, Moon proved that passive damping methodology using piezoelectric materials with resonant circuit can effectively attenuate the flutter. (Moon et al., 2002) In the same context, it is still correct to say that there is a need and a considerable interest in alternative methods of increasing the flutter speed beyond the original unaided value. All these facts fully underline the necessity of the implementation of an active control capability enabling one to fulfil two basic objectives : a) to enhance the subcritical aeroelastic response, in the sense of suppressing the wing oscillations in the shortest possible time, and b) to extend the flight envelope by suppressing flutter instability and so, of contributing to a significant increase of the allowable flight speed. With this in mind, in this paper the active aeroelastic control of a 3-DOF (three degree of freedom) wing system exposed to an incompressible flowfield will be investigated. The aeroelastic model adopted herein is that of a thin air foil immersed in a nonviscous, unsteady incompressible flowfield. This model is able to capture most of the dynamics of a three dimensional wing and for this reason is still well used in linear and nonlinear analysis. (Horikawa and Dowell, 1979 ; Vipperman et al., 1998)

In the last two decades, the advances of the active control technology have rendered the applications of active flutter suppression and active vibrations control systems feasible. (Horikawa and Dowell, 1979 ; Lazaraus et al., 1995) In a classical sense, the active flutter and vibration suppression control is adopted by employing a control surface as a primary control. Its deflection is commanded by a suitable control law, i.e. by a relationship between the motion of the 2-D wing section and the control surface deflection. However, due to unmeasurable aerodynamic lag states, developing an active control using full-state feedback is not viable. The use of a state-estimator is a more practical way of developing active controllers. In the present paper, both negative velocity feedback control methodology and LQG scheme are implemented, and some of their performances are put into evidence. Even though LQG method gives better performance as expected, we continue discussing velocity feedback control, as the LQG would require six sensors to implement in this case, while velocity feedback control requires only one. (Shim and Na, 2003) From a physical point of view, the active control is achieved by deflecting the control surface in a manner that alters the overall nature of the aerodynamic forces on the wing, as to change in a beneficial way the dynamics of the wing structure.

In the present paper, the aerodynamic forces are used for the case of time-dependent arbitrary motions of a 3 DOF airfoil featuring plunging-pitching-flapping deflections, which are derived from the Theodorsens equations using Wagner's function. (Edwards, 1977)

In spite of the interest and intense research work concerning modeling and analysis for the

effects of the characteristic parameters of explosive pressures such as sonic-boom and blast loads through the atmosphere to wing-type structures, few results concerning the aeroelastic response to various loads can be found in the specialized literature. It should be noted that the time domain formulation of the lifting surfaces is essential towards determination of the dynamic aeroelastic response to time-dependent external loads. The principal goal of the paper is that of investigating in the subcritical aeroelastic response of 3-DOF wing type surfaces to gust and explosive loads associated with uncontrolled/controlled mode. To this end, a conventional control methodology using negative velocity feedback control law and the Linear Quadratic Gaussian (LQG) method are implemented and their performances toward enhancing the aeroelastic response in the subcritical flight speed range are demonstrated.

2. Configuration of the 3-DOF Wing-Flap Model

Figure 1 shows the typical airfoil-flap section that is considered in the present analysis. The 3-DOF configuration associated with the airfoil appears clearly from Fig. 1. In order to provide the proper restraining forces so that the airfoil behaves as part of an attached wing, one assumes the existence of linear and torsional springs. (Scanlan and Rosenbaum, 1951 ; Edwards, 1977) The stiffness coefficients for these springs are given by K_h and K_α, respectively. The torsional flap spring with stiffness coefficient K_β provides a restraining force on the control flap. The control force is given by a torque applied to this spring. The plunge displacement is denoted by h, the pitch angle, α and the flap angle of the controlling flap, β. The plunge is measured positive downward. The pitch, or the angle of attack, is measured from the horizontal at the elastic axis of the airfoil, positive nose-up.

The flap angle is measured from the axis created by the airfoil at the control flap hinge, positive flap-down.

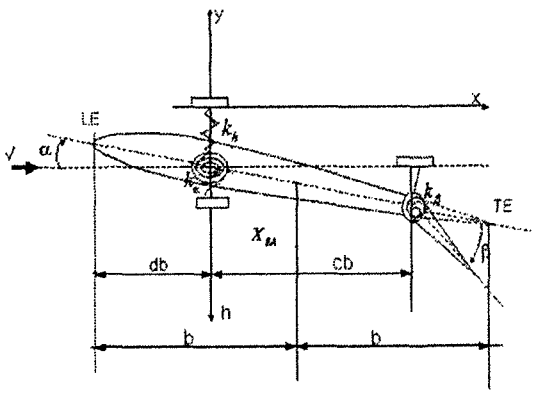

Fig. 1 3-DOF wing-flap section

3. Governing Equations of the Aeroelastic System Model

The governing equations pertinent to the 3-DOF aeroelastic systems can be found in the classical aeroelasticity monographs (Edwards, 1977 ; Olds, 1997). In matrix form the equations governing the aeroelastic motion of a 3-DOF wing system can be written as : (Olds, 1997 ; Bail, 1997)

$$\mathbf{M}\ddot{\mathbf{Y}}(t)+\mathrm{KY}(t)=-[L_T(t)\ M_T(t)\ T_T(t)]^T \quad (1)$$

In this equation the column vector of plunging/pitching/flapping displacements is defined as

$$\mathbf{Y}(t)=[h(t)\ \alpha(t)\ \beta(t)]^T \quad (2)$$

where

$$\mathbf{M}=\begin{bmatrix} m & S_\alpha & S_\beta \\ S_\alpha & I_\alpha & I_\beta+bcS_\beta \\ S_\beta & I_\beta+bCS_\beta & I_\beta \end{bmatrix} \quad (3)$$

$$\mathbf{K}=\begin{bmatrix} K_h & 0 & 0 \\ 0 & K_\alpha & 0 \\ 0 & 0 & K_\beta \end{bmatrix} \quad (4)$$

denote the mass and stiffness matrices, respectively.

The second order aeroelastic governing equation can be cast in a first order state-space form in order to implement various feedback control laws as :

$$\dot{\mathbf{X}}(t)=\mathbf{AX}(t)+\mathbf{Bu}(t)+\mathbf{Gw}(t) \quad (5)$$

The state vector X(t) is given by

$$\mathbf{X}(t)=[\dot{h}(t)\ \dot{\alpha}(t)\ \dot{\beta}(t)\ h(t)/b\ \alpha(t)\ \beta(t)\ B_1(t)\ B_2(t)\ A_1(t)\ A_2(t)]^T \quad (6)$$

where the last four states, $B_1(t)$, $B_2(t)$, $A_1(t)$ and $A_2(t)$, are the aerodynamic lag states. The control input $u(t)$ is the torque applied to the flap. The input $\mathbf{w}(t)$ is an external disturbance represented by a time-dependent external excitation, such as gust; **G** is the disturbance-input matrix, while **B** is the control input matrix that is given by

$$\mathbf{B}=\frac{1}{I_\beta}[(\mathrm{M}^{-1}[0\ 0\ 1]^T)^T\ 0\ 0\ 0\ 0\ 0\ 0\ 0]^T \quad (7)$$

4. Time-Dependent Loads Associated with Aerodynamic Loads and Explosive Loads

4.1 Configuration of the aerodynamic loads

The aerodynamic load vector appearing in Eq. (1) is expressed in terms of its components as

$$L_T(t)=L(t)+L_G(t) \quad (8)$$

$$M_T(t)=M(t)+M_{yG}(t) \quad (9)$$

$$T_T(t)=T(t)+T_{yG}(t) \quad (10)$$

where L, M and T denote the aerodynamic lift (positive in the upward direction), the pitching moment about the one-quarter chord of the airfoil (positive nose-down), and the flap torque applied to the flap hinge, respectively.

The second terms of the right sides in the expressions (5)-(7) are due to the wind gust. In this respect, for the gust loading we have (Dowell, 1978):

$$L_G(t)=\int_0^t I_{LG}(t-\sigma)\frac{w_G}{V}\,d\sigma \quad (11)$$

$$M_{yG}(t)=\int_0^t I_{MG}(t-\sigma)\frac{w_G}{V}\,d\sigma \quad (12)$$

$$T_{yG}(t)=\int_0^t I_{fG}(t-\sigma)\frac{w_G}{V}\,d\sigma \quad (13)$$

where I_{LG}, I_{MG} and I_{fG} are the related indicial impulse functions. For the incompressible flow, we have:

$$I_{LG}=4\pi\psi \quad (14)$$

$$I_{MG}=I_{LG}(1/2+x_{XA}/b) \quad (15)$$

$$I_{fG}=0 \quad (16)$$

The Kssner's function ψ is a approximated by:

$$\psi(t)=1-0.5e^{-0.13t}-0.5e^{-t} \quad (17)$$

In the time domain, aerodynamic loads have the forms as follows:

$$L(t)=\pi\rho b^2\Big[\ddot{h}(t)-ba\ddot{\alpha}(t)+\frac{b}{2\pi}\Phi_4\ddot{\beta}(t)+V\dot{\alpha}(t)+\frac{V}{\pi}\Phi_3\dot{\beta}(t)\Big]+2\pi\rho VbD(t) \quad (18)$$

$$M(t)=\pi\rho b^3\Big[-a\ddot{h}(t)+b\Big(\frac{1}{8}+a^2\Big)\ddot{\alpha}(t)+\frac{b}{4\pi}\Phi_7\ddot{\beta}(t)+\Big(\frac{1}{2}-a\Big)V\dot{\alpha}(t)+\frac{V}{2\pi}\Phi_6\dot{\beta}(t)\frac{V^2}{\pi b}\Phi_5\beta(t)\Big]-2\pi\rho b^2\Big(\frac{1}{2}+a\Big)VD(t) \quad (19)$$

$$T(t)=\pi\rho b^2\Big[\Big(\frac{b}{2\pi}\Phi_4\Big)\ddot{h}(t)+\Big(\frac{b^2}{4\pi}\Phi_7\Big)\ddot{\alpha}(t)+\Big(\frac{b^2}{2\pi^2}\Phi_{12}\Big)\ddot{\beta}(t)+\Big(\frac{bV}{2\pi}\Phi_9\Big)\dot{\alpha}(t)+\Big(\frac{bV}{2\pi^2}\Phi_{11}\Big)\beta(t)+\Big(\frac{V^2}{\pi^2}\Phi_{10}\Big)\beta(t)\Big]+\pi\rho VbP(t) \quad (20)$$

The functions $D(t)$ and $P(t)$ are Duhamel Integrals given in Appendix A.

4.2 Gust, blast and sonic-boom pulses

Herein, the response of 3-DOF wing system to gust, explosive blast and sonic boom overpressure signatures will be addressed. In the following developments, Küssner's function derived for sharp-edged gusts will be used to determine the aeroelastic response to gusts of different shapes. In this context, gusts of selected shapes, implying specific time variations of their velocity distribution will be used. Such distributions used in this study are: (a) sharp-edged gust (Fig. 2 (a)), (b) 1-COSINE gust (Fig. 2(b)), (c) triangular gust (Fig. 2(c)) and (d) graded gust (Fig. 2(d)). Their analytical expressions are:

sharp-edged gust : $\omega_G(\tau)=H(\tau)\,\omega_0$

1-COSINE gust :

$$\omega_G(\tau)=H(\tau)\frac{1}{2}\,\omega_0\left(1-\cos\frac{\pi\tau}{\tau_G}\right)-H(\tau-2\tau_G)\frac{1}{2}\,\omega_0\left(1-\cos\frac{\pi\tau}{\tau_G}\right)$$

triangular gust :

$$\omega_G(\tau)=2\omega_0\frac{\tau}{\tau_G}\left(H(\tau)-H\left(\tau-\frac{\tau_G}{2}\right)\right)-2\omega_0\left(\frac{\tau}{\tau_G}-1\right)\left(H(\tau-2\tau_G)-H\left(\tau-\frac{\tau_G}{2}\right)\right) \tag{21}$$

graded gust : $\omega_G(\tau)=H(\tau)=\omega_0(1-e^{-0.75t})$

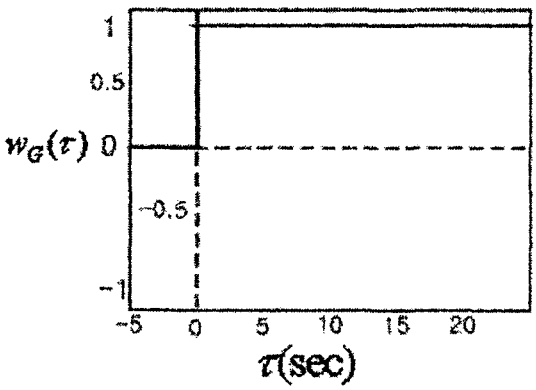

(a)

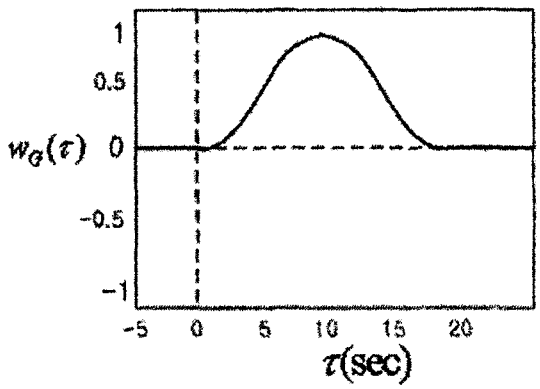

(b)

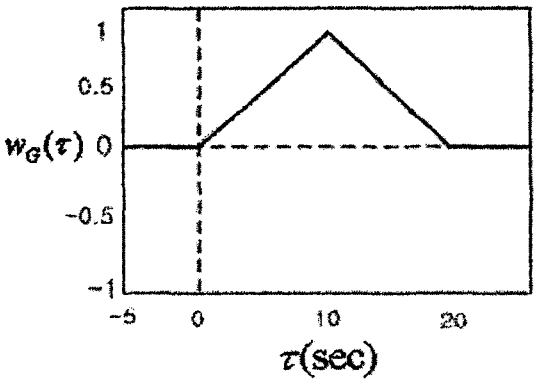

(c)

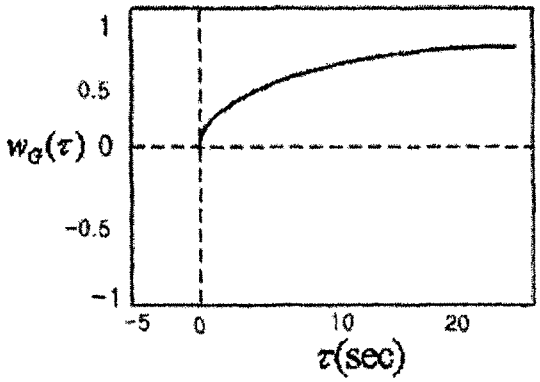

(d)

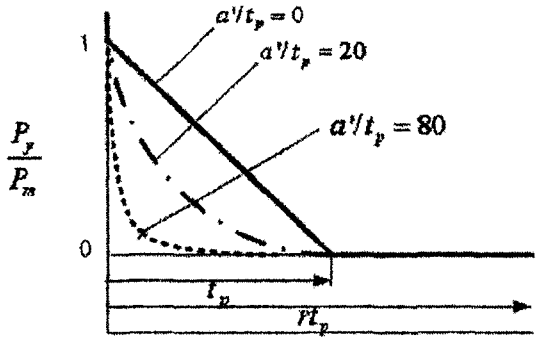

(e)

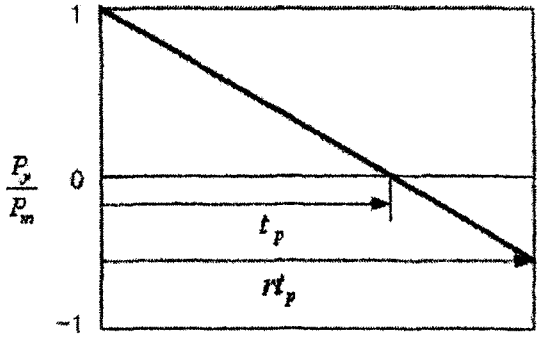

(f)

Fig. 2 (a) Sharp-edged gust (b) 1-COSINE gust (c) Triangular gust (d) Graded gust (e) Blast load (f) Sonic-boom

Herein, the Heaviside step function $H(\tau)$ has been introduced to describe the typical velocity distribution corresponding to the various types of gust load. For the case of blast loadings, various analytical expressions have been proposed and discussed (see, e.g., Gupta, 1985; Birman and Bert, 1987). As it was clearly shown based on experimental evidence, the blast wave reaches the peak value in a short time and can be described in terms of the modified Friedlander exponential decay equation as:

$$P_y=P_m\left(1-\frac{t}{t_p}\right)e^{-a't/t_p} \tag{22}$$

where P_m denotes the peak reflected pressure, t_p denotes the positive phase duration of the pulse and a' represents a decay parameter which has to be adjusted to approximate the overpressure signature. A depiction of the ratio P_y/P_m vs time for various values of the ratio a'/t_p and a fixed value of t_p is displayed in Fig. 2(e). Regarding the sonic-boom loadings, it can be modeled as an N-shaped pressure pulse arriving at a normal incidence. Such a pulse may be produced by an aircraft flying supersonically in the earth's atmosphere or by any supersonic projectile rocket or missile. The N-wave shock pulse can be described by

$$P_y=\begin{cases} P_m\left(1-\dfrac{t}{t_p}\right) & \text{for } 0<t<rt_p \\ 0 & \text{for } t>rt_p \end{cases} \tag{23}$$

where r denotes the shock pulse length factor, and P_m and t_p maintain the same meaning as in the case of blast pulses. It may easily be seen that i) for $r=1$ the N-shaped pulse degenerates into a triangular pulse; ii) for $r=2$ a symmetric N-shaped pressure pulse is obtained; while iii) for $1<r<2$ the N-shaped pulse becomes an asymmetric one as shown in Fig. 2(f).

5. Design of Control Methodology and Stability Analysis

Within the present simulations, a standard negative velocity feedback control law and LQG control law will be applied, respectively. In the present case, due to the fact the proportional and acceleration controls were proven to be less efficient, only combined velocity feedback control will be addressed. As a result, herein, plunging/pitching velocity feedback control and their combinations are used. These relates the control input $\mathrm{u}(t)$, i.e., the required flap deflection angle, to the decoupled plunging and pitching velocities of the main airfoil surface. Hence $\mathrm{u}(t)$ is represented according to the law

$$\mathrm{u}(t)=-g_h(\dot{h}/b)-g_a(\dot{\alpha}) \tag{24}$$

Herein g_h and g_a are the corresponding control gains.

In the context of optimal control law, a Linear Quadratic Regulator (LQR) technique is initially used where the optimal regulator problem is to find a control input $\mathrm{u}(t)$, which drives the states $\mathrm{X}(t)$ to zero in an arbitrarily short time. The optimal full-state feedback gain required to achieve this task is obtained by minimizing a scalar performance index (Na and Librescu, 2000)

$$\begin{aligned} J&=\int_0^{t_f}[\mathrm{X}^{\mathrm{T}}\mathrm{Z}\mathrm{X}+\mathrm{u}^{\mathrm{T}}\mathrm{R}\mathrm{u}]\mathrm{d}t \\ &=\int_0^{t_f}[\dot{\mathrm{q}}^{\mathrm{T}}\mathrm{M}\dot{\mathrm{q}}+\mathrm{q}^{\mathrm{T}}\mathrm{K}\mathrm{q}+\mathrm{u}^{\mathrm{T}}\mathrm{R}\mathrm{u}]\mathrm{d}t \end{aligned} \tag{25}$$

where

$$\mathrm{Z}=\begin{bmatrix}\mathrm{K} & 0\\ 0 & \mathrm{M}\end{bmatrix} \tag{26}$$

Note that the state weighting matrix Z was chosen so that the first term in the cost function represents the sum of the system kinetic and potential energies.

Herein if the terminal time t_f approaches infinity, the Riccati gain matrix $P(t)$ becomes a constant $\mathrm{P_C}$ which is the solution to the nonlinear algebraic Riccati equation.

$$\mathrm{A}^{\mathrm{T}}\mathrm{P_C}+\mathrm{P_C}\mathrm{A}-\mathrm{P_C}\mathrm{B}\mathrm{R}^{-1}\mathrm{B}^{\mathrm{T}}\mathrm{P_C}+\mathrm{Z}=0 \tag{27}$$

The optimal controller for the controlled system can be obtained in this case as

$$\mathrm{u}(\mathrm{t})=-\mathrm{R}^{-1}\mathrm{B}^{\mathrm{T}}\mathrm{P_C}(\mathrm{t})\,\mathrm{X}(\mathrm{t}) \tag{28}$$

and

$$|\mathrm{u}(\mathrm{t})|<\mathrm{u_{max}} \tag{29}$$

where $\mathrm{u_{max}}$ represents the maximum control input.

While the LQR design provides a robust controller, the unavailability of all states for feedback makes the design impracticable. In this respect, an LQG design, which uses noise-corrupted outputs for feedback, is used as a controller. The practicality of the LQG design also lies in the assumption that the uncertainty is represented as an additive white noise. It is assumed that additive process noise v and the measurement noise n are uncorrelated zero-mean, Gaussian, white-noise. The corresponding state space equations are given by

$$\dot{\mathbf{X}}(t)=\mathbf{AX}(t)+\mathbf{Bu}(t)+\mathbf{Gw}(t)+v(t) \quad (30a)$$

$$y=\mathbf{C}\,\mathbf{X}+n(t) \quad (30b)$$

where y is a measured output while v, the plant noise and n, the measurement noise are white and Gaussian with joint correlation function

$$G\left(\begin{bmatrix}v(t)\\ n(t)\end{bmatrix}[v(t)\,n(t)]\right)=\begin{bmatrix}V & 0\\ 0 & W\end{bmatrix}\delta(t-\tau) \quad (31)$$

For the present case, V and W are defined to be

$$V=[I_{10\times10}], \text{ and } W=[I_{6\times6}]$$

The associated control input is obtained such that the system is stabilized and the control minimizes the cost function

$$J_{LQG}=\lim_{T\to\infty} E\left\{\int_0^T [X(t)^T u(t)^T]\begin{bmatrix}Z & 0\\ 0 & R\end{bmatrix}\begin{bmatrix}X(t)\\ u(t)\end{bmatrix}dt\right\} \quad (32)$$

The matrice Z is defined earlier and R is defined to be

$$R=\alpha I \quad (33)$$

Herein α is a scaling factor and I is an identity matrix.

The LQG design methodology is a combination of LQR and a Kalman filter as the state estimator. In LQG design the measured output is used to build a state estimator for the system. This state estimator is of the form (Dorato et al., 1995)

$$\frac{d}{dt}\hat{X}[A+LC]\hat{X}-Ly+Bu(t) \quad (34)$$

The control law makes use of this estimator and is defined by

$$u(t)=-X_c\hat{X} \quad (35)$$

The control gain K_c and the filter gain L are defined as, respectively (Dorato et al., 1995)

$$K_c=-R^{-1}B^TP_c \quad (36)$$

and

$$L=-\Pi C^T W^{-1} \quad (37)$$

Hence, we expect that u(t) stabilize the system much like LQR utilizing full-state feedback. The LQG controller is built by first solving the decoupled algebraic Riccati equations

$$A^TP_c+P_cA-P_cBR^{-1}B^TP_c+Z=0 \quad (38)$$

$$A\Pi+\Pi A^T-\Pi C^T W^{-1}C\Pi+V=0 \quad (39)$$

6. Results and Discussions

The considered geometrical characteristics of the 3-DOF wing system are used in the work by Edwards (1977), of which corresponding data are shown in Table 1, and the associated flutter speed is $V_F=271.3$ m/sec.

The critical value of the flutter speed is obtained herein via the solution of both the complex eigenvalue problem and from the subcritical aeroelastic response analysis. The flutter characteristics obtained via the present approach, are in excellent agreement with Edwards (1977) and Olds (1997). In the presence of external time-dependent excitations, the determination of the time history of the response quantities ($\hat{h}$, α, β), at any flight speed lower than the flutter speed, requires the solution of a boundary-value problem (Na and Librescu, 1998). $\hat{h}(\equiv h/b)$ denotes

Table 1 Geometrical characteristics of the 3-DOF wing system

b=0.9144(m)	$K_h=50^2$ m
$x_{EA}=-0.4$	$K_\alpha=100^2 I_\alpha$
c=1.0	$K_\beta=300^2 I_\beta$
$m=128.6820\left(\frac{kg}{m}\right)$	$\rho=1.2252\left(\frac{kg}{m^3}\right)$
$I_\beta=0.672466\left(\frac{kg-m^2}{m}\right)$	$S_\beta=1.4706$(kg)
$S_\alpha=23.53333$(kg)	$I_\alpha=26.8280\left(\frac{kg-m^2}{m}\right)$

nondimensionalized plunging displacement. Furthermore, Figure 3 depicts the variations of flutter speed V_F, against velocity feedback gains g_h and g_α. The result reveals that the flutter speed increases in a certain range with the increase of the feedback gain until a maximum value, beyond which a sharp drop of the flutter speed is experienced. The nominal point of the g_α occurs farther after the one of the g_h, which is not shown in the result. The similar trend of both authority and limitation of the velocity feedback gain is also found in Shim and Na (2003). The aeroelastic stability characteristics are obtained by finding the eigenvalues of the corresponding characteristic equation of Eq. (1). The results of the aeroelastic stability analysis are presented in the form of root loci, where the solution (which are complex eigenvalues) at each flight speed is plotted on real/imaginary plane. In the same context, Figs. 4(a) and 4(b) display the root locus of the only fifth pole related to pitching motion (dominant role in the present case) upon which plunging/pitching velocity feedback control applied, respectively. In Fig. 4(a), one can observe that the path of the pole mainly exist at right half plane (RHP) of the domain even though the value of the control gain g_h increases, which reveals plunging velocity feedback seems not to be possible to reduce the aeroelastic response except narrow band associated with flight speeds and control gains. However, Fig. 4(b) indicates that the pole moves to the left half plane from the RHP when the pitching control gain increases, which shows strongly positive effect with an increase of the flight speed. In this regard, it should be stressed again that the result clearly shows a complete understanding of the influence of feedback mechanism authority; the pitching velocity gain g_α works better than the counterpart of it, plunging velocity feedback gain g_h, in the point of capability of increasing flutter speed.

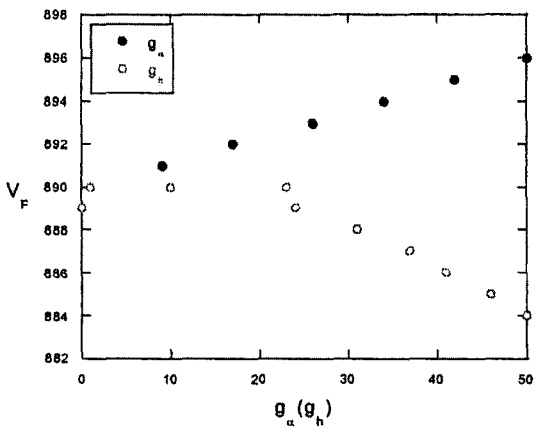

Fig. 3 Variations of flutter speed vs. velocity feedback gains

The aeroelastic response time-histories of a 3-DOF wing-flap system subjected to gust loads and explosive time-dependent external excitations are displayed in Figs. 5-9. The plots depic-

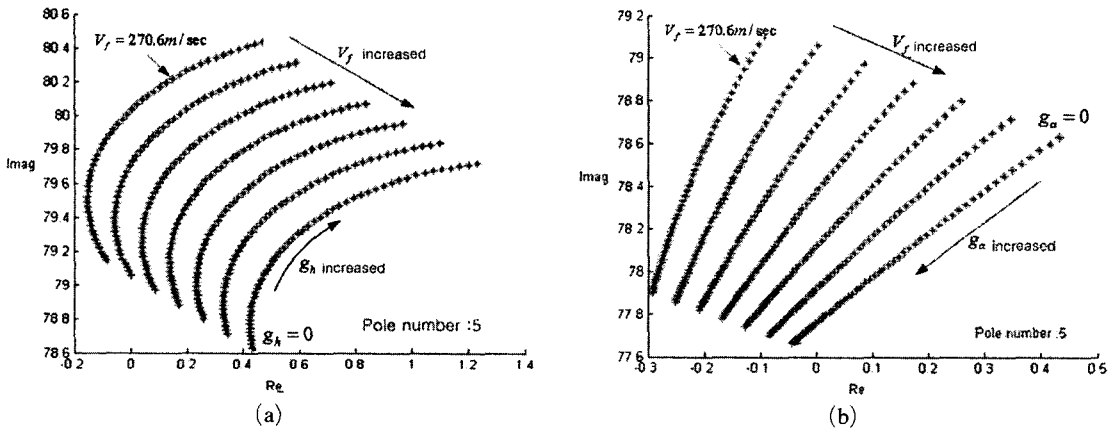

Fig. 4 Root locus of the fifth pole of the closed system upon plunging/pitching velocity feedback gain applied

ting the aeroelastic response time-histories $\hat{h}$, α of the aeroelastic system to blast load are displayed in Figs. 5(a), (b). Those figures show that with the decrease of the parameter a', higher amplitude of the deflection are obtained. It should be indicated that the specific condition such as variation of parameter, a'/t_p in the blast load is the dramatic role on the associated aeroelastic response of the wing system. Figures 5(c), (d) display the aeroelastic response $\hat{h}$, α of the system subjected to sonic-boom pressure pulses, which reveals the quantitative and qualitative differences in the aeroelatic response due to a symmetric ($r=2$) and asymmetric ($r=1.5$) N-shaped pulse. It should be pointed that corresponding to the specific conditions such as variation of parameter, r, the response to sonic-boom pressure pulse features two distinct time periods; one for $0<\tau<rt_p$, that corresponds to the forced motion regime, and the other one for $\tau>rt_p$, belonging to the free motion regime. The jump in the time-history of N-shaped sonic-boom is due to the discontinuity in the load occuring at $\tau=rt_p$. This jump does not appear in the time-histories of the explosive pressure pulses, where $r=1.0$.

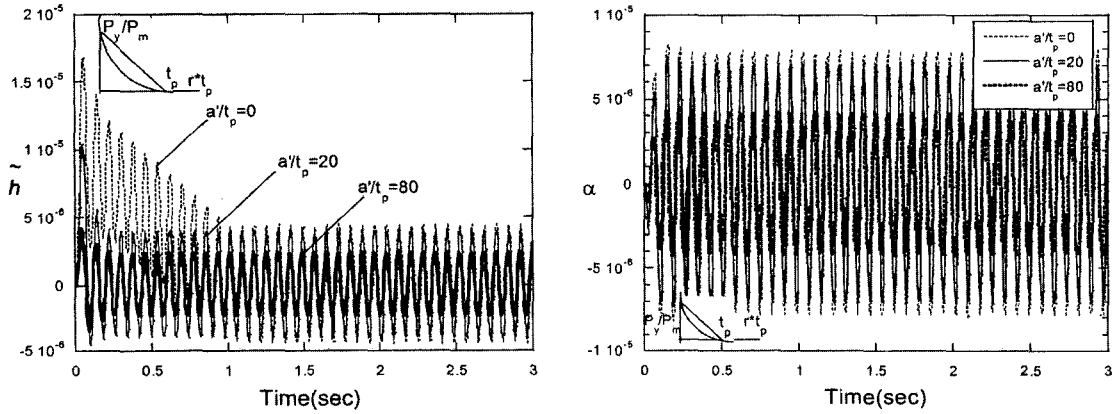

Fig. 5(a) (b) The dimensionless plunging/pitching response time-histories subjected to blast loading in terms of a'/t_p

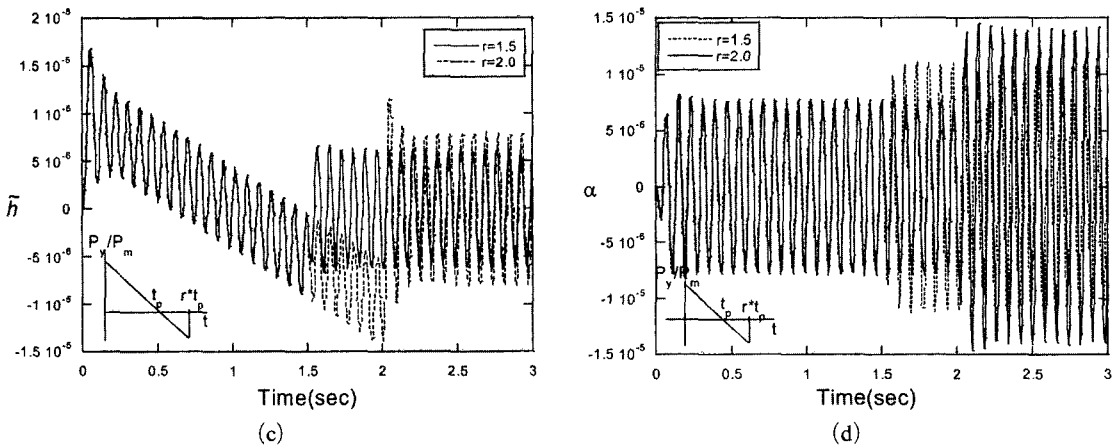

Fig. 5(c) (d) The dimensionless plunging/pitching response time-histories subjected to sonic-boom in terms of parameter r

Figure 6(a) and 6(b) display the open/closed dimensionless response time-histories of the quantities, $\hat{h}$, α of the aeroelastic system operating in close to the flutter boundary (V=270.96 m/sec) subjected to the graded gust (represented in the inset of the respective figures). The results show that the amplitudes of the corresponding response are on the verge of increasing in time, implying that the system is in close proximity to the flutter instability. However, the application of the LQG to stabilize the plunging/pitching aeroelastic response of the airfoil appears to be successful. The open/closed dimensionless aeroelastic responses to blast loads corresponding plunging and pitching motion are depicted in Figs. 7(a) and 7(b), respectively. The result shows that within the free motion regime (i.e. for $t>10$ sec) the implemented control methodology is much more effective than within the forced motion regime. The open/closed-loop system exposed to a sonic-boom (r=2.0) are depicted in Figs. 8(a) and 8(b). From the graph, the authority of the adopted control law becomes fully evident again. Figures 9(a) and 9(b) show that the open/closed nondimensionalized aeroelastic response to sharp-edged gust, at two different flight speeds V= 243.84 m/sec, $V=V_F$. It becomes apparent that the amplitude of the aeroelastic response de-

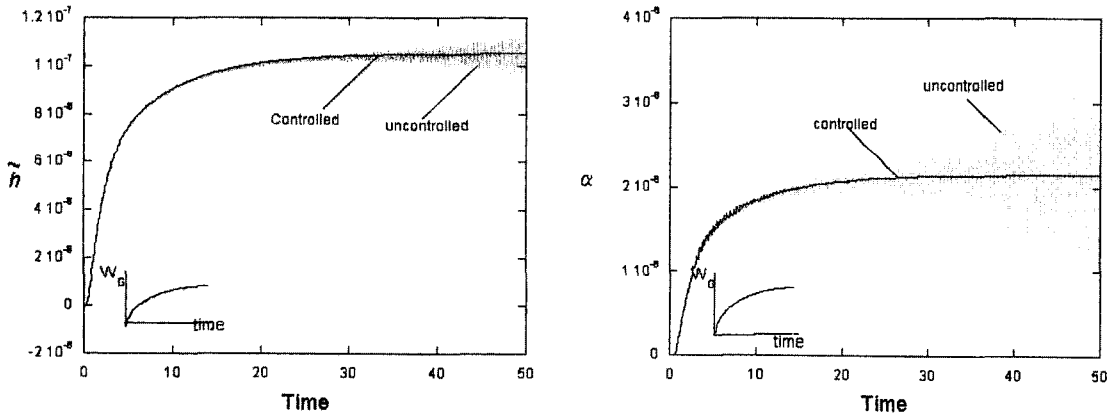

(a) (b)

Fig. 6 The open/closed dimensionless plunging/pitching response time-histories to graded gust (V_f=270.96 m/sec)

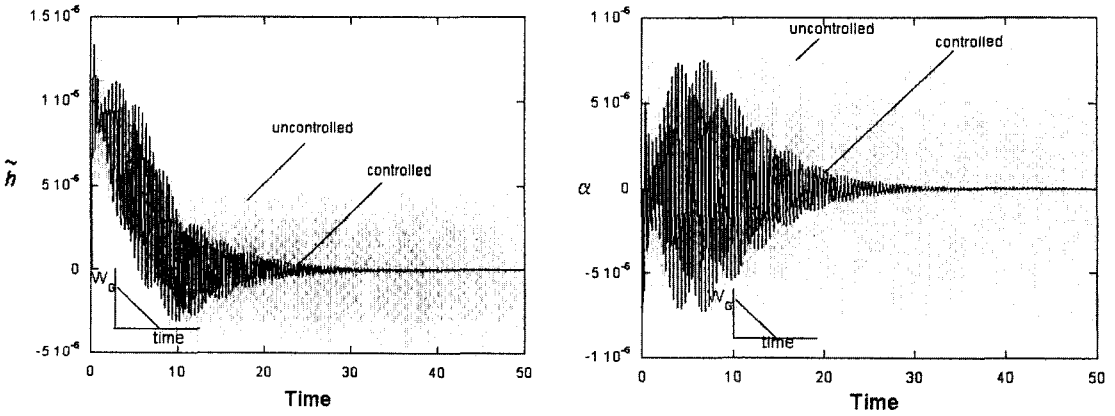

(a) (b)

Fig. 7 The open/closed dimensionless plunging/pitching response time-histories to balst

creases with the increase of the speed. However, for $V=V_F$ the response becomes unbounded, implying that the occurrence of the flutter instability is impending. In this connection, whereas for flight speeds below the flutter speed, a very little influence of the control is visible, in the sense of a marginal influence on the time-history, at $V\approx V_F$ the flutter response is converted, by control action, a stable response.

7. Conclusions

In this paper, the aeroelastic response and control of 3-DOF wing-flap systems operating in an incompressible, subcritical flight speed and exposed to explosive time-dependent loads and gust loads are presented. The paper also illustrates the methodology and the importance of the implementation of the active control synthesis on the lifting surface equipped with a flap. The closed-loop equation of motion for the wing-flap system is derived and the corresponding complex eigenvalue problem as well as aeroelastic response problem is solved numerically. To the best of the authors' knowledge no results concerning subcritical open/closed aeroelastic response of the 3-DOF wing systems subjected to blast and sonic-boom pressure signatures are available in the

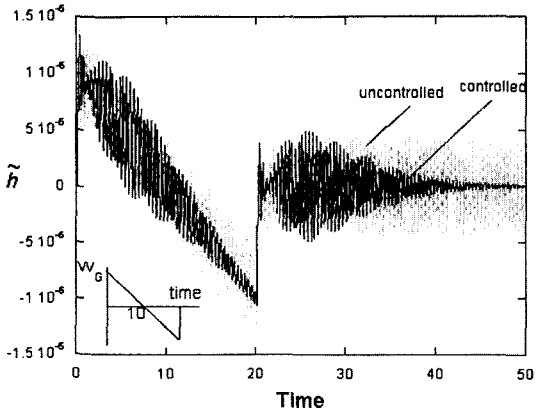

Fig. 8(a) The counterparts of Fig. 6(a) for a sonic-boom ($r=2.0$)

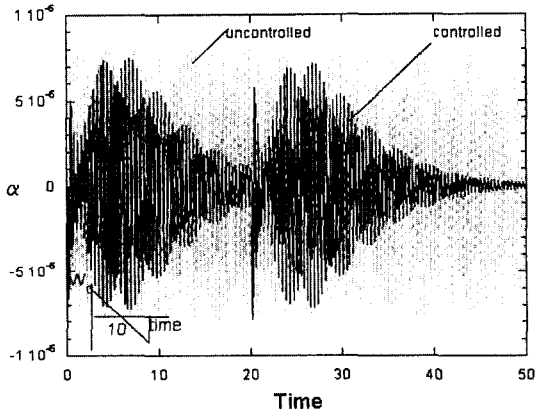

Fig. 8(b) The counterparts of Fig. 6(b) for a sonic-boom ($r=2.0$)

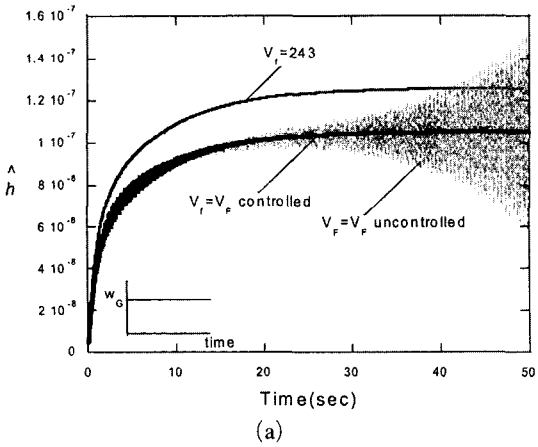

(a)

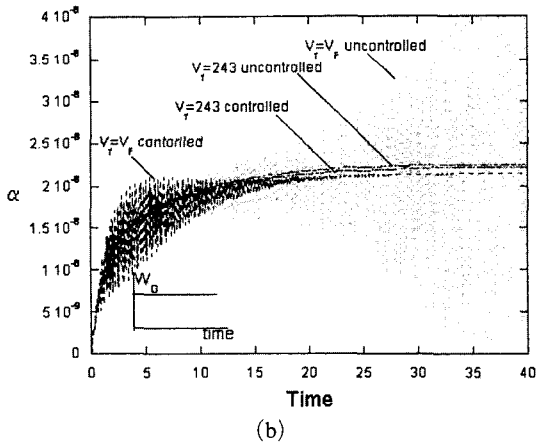

(b)

Fig. 9 The open/closed dimensionless plunging/pitching response time-histories to sharp-edged gust at two different flight speeds. ($V_f=243.83$ m/sec, $V_f=V_F$)

specialized literature.

Acknowledgment

Sungsoo Na acknowledges the support by the Basic Research Program of the Korea Science & Engineering Foundation, Grant No. R01-2002-000-00129-0.

References

Bail, T. R., 1997, "A Disturbance Rejection Problem for a 2-D Airfoil," MS Thesis, Department of Mathematics, Mathematics, Virginia Polytechnic Institute and State University, Blackburg, VA.

Birman, V. and Bert, C. W., 1987, "Behavior of Laminated Plates Subjected to Conventioal Blast," *Int. J. Impact Eng.*, Vol. 6, No. 3, pp. 145~155.

Dorato, P., Abdallah, C. and Cerone, V., 1995, *Linear-Quadratic Control*, Prentice Hall.

Dowell, E. H., 1978, *A Modern Course in Aeroelasticity*, Sijthoff and Noordhoff.

Edwards, J. W., 1977, "Unsteady Aerodynamic Modeling and Active Aeroelastic Control," SUDARR 504 (NASA Grant ngl-05-020-007), Stanford University, Feb. 1977. Also available as NASA CR-148019.

Gupta, A. D., 1985, "Dynamic Analysis of a Flat Plate Subjected to an Explosive Blast," *Proc. ASME Int. Computers Eng. Conf.* 1, pp. 491~496.

Horikawa, H. and Dowell, E. H., 1979, "An Elementary Explanation of the Flutter Mechanism with Active Feedback Controls," *Journal of Aircraft*, Vol. 16, No. 4, pp. 225~232.

Lazaraus, K., Crawley, E. and Lin, C., 1995, "Fundamental Mechanism of Aeroelastic Control with Control Surface and Strain Actuation," Journal of Guidence, Control, and Dynamics, Vol. 18, No. 1, pp. 10~17.

Marzocca, P., Librescu, L. and Chiocchia, G., 2001, "Aeroelastic Response of a 2-D Lifting Surface to Gust and Arbitrary Explosive Loading Signatures," *International Journal of Impact Engineering*, Vol. 25, No. 1, pp. 41~65.

Marzocca, P., Librescu, L. and Chiocchia, G., 2002, "Aeroelasticity of Two-Dimensional Lifting Surface Via Indical Function Approach," *The Aeronautical Journal*, pp. 147~153.

Marzocca, P., Librescu, L. and Chiocchia, G., 2002, "Aeroelastic Response of a 2-D Airfoil in Compressible Flight Speed Regimes Exposed to Blast Loadings," *Aerospace Science and Technology*, Vol. 6, No. 4, pp. 259~272.

Marzocca, P., Librescu, L. and Silva, W. A., 2002, "Flutter, Post-Flutter and Control of a Supersonic 2-D Lifting Surface," *Journal of Guidence, Control, and Dynamics*. Vol. 25, No. 5, pp. 962~970.

Moon, S. H., Yun, C. Y. and Kim, S. J., 2002, "Passive Suppression of Nonlinear Panel Flutter Using Piezoelectric Materials with Resonant Circuit," *KSME International Journal*, Vol. 16, No. 1, pp. 1~12

Na, S. S. and Librescu, L., 2000, "Optimal Vibration Control of a Thin-Walled Anisotropic Cantilevers exposed to Blast Loading," *Journal of Guidance, Control and Dynamics*, 23, pp. 491~500.

Olds, S. D., 1997, "Modeling and LQR Control of a Two-Dimensional Airfoil," MS Thesis, Department of Mathematics, Virginia Polytechnic Institute and State University, Blackburg, VA.

Scanlan, R. H. and Rosenbaum, R., 1951, *Introduction to the study of Aircraft Vibration and Flutter*, The Macmillian Co..

Shim, J. K. and Na, S. S., 2003, "Modeling and Vibration Feedback Control of Rotating Tapered Composite Thin-Walled Blade," *KSME International Journal*, Vol. 17, No. 3, pp. 380~390.

Vipperman, J. S., Clark, R. L., Conner, M. D. and Dowell, E. H., 1998, "Investigation of the Experimental Active Control of a Typical Section Airfoil Using a Trailing Edge Flap," *Journal of Aircraft*, Vol. 35, No. 2, pp. 224~229.

Yoo, N., 2001, "Aerodynamic Performance Improvement by Divergent Trailing Edge Modification to a Supercritical Airfoil," *KSME International Journal*, Vol. 15, No. 10, pp. 1434~1441.

York, D. L., 1980, "Analysis of Flutter and Flutter Suppression via Energy Method," MS Thesis, Department of Aerospace and Ocean

Engineering, Virginia Polytechnic Institute and State University, Blacksburg, VA.

Appendix A

The functions $D(t)$ and $P(t)$ are Duhamel Integrals given by

$$D(t)=\int_0^t \Phi\left[\frac{(t-\sigma)\,V}{b}\right]Q_i'(\sigma)\,d\sigma \tag{A1}$$

$$P(t)=\int_0^t \Phi\left[\frac{(t-\sigma)\,V}{b}\right]Q_2'(\sigma)\,d\sigma \tag{A2}$$

where $\Phi\left[\frac{(t-\sigma)\,V}{b}\right]$ is the Wagner's function whose argument is $\frac{(t-\sigma)\,V}{b}$.

$$\begin{aligned}Q_1'(\tau)=\frac{dQ_1(\tau)}{d\tau}&=h''(\tau)+\alpha''(\tau)\,b\\&+\frac{b}{2\pi}\Phi_2\beta''(\tau)+V\alpha'(\tau)+\frac{V}{\pi}\Phi_1\beta'(\tau)\end{aligned} \tag{A3}$$

$$\begin{aligned}Q_2'(\tau)=\frac{dQ_2}{d\tau}&=\frac{b}{\pi}\Phi_8h''(\tau)+\frac{b^2}{\pi}\Phi_8\alpha''(\tau)\\&+\frac{b^2}{2\pi^2}\Phi_2\Phi_8\beta''(\tau)+\frac{Vb}{\pi}\Phi_8\alpha'(\tau)\\&+\frac{Vb}{\pi^2}\Phi_1\Phi_8\beta'(\tau)\end{aligned} \tag{A4}$$

$$\tau=t\,\frac{V}{b} \tag{A5}$$

While $\Phi_i(\phi)$ are Theodorsen's Constants, where $\phi=\arccos(-x_{flap}/b)$.

The standard two-term Jones exponential approximation of the Wagenr's function is given by

$$\begin{aligned}&\Phi(\tau)=1-\alpha_1e^{-\beta_1\tau}-\alpha_2e^{-\beta_2\tau}\,;\\&\alpha_1=0.165\,;\ \alpha_2=0.335\,;\ \beta_1=0.041\,;\ \beta_2=0.32\end{aligned} \tag{A6}$$

By replacing Eq. (A-6) in Eqs. (18) and (20), one obtain for $D(t)$ and $P(t)$ the expressions:

$$D(t)=Q_1(t)-\alpha_1B_1(t)-\alpha_2B_2(t) \tag{A7}$$

$$P(t)=Q_2(t)-\alpha_1A_1(t)-\alpha_2A_2(t) \tag{A8}$$

where

$$\begin{aligned}Q_1(t)=\dot h(t)+\dot\alpha(t)\,b+\frac{b}{2\pi}\Phi_2\dot\beta(t)\\+V\alpha(t)+\frac{V}{\pi}\Phi_1\beta(t)\end{aligned} \tag{A9}$$

$$\begin{aligned}Q_2(t)=\frac{b}{\pi}\Phi_\pi\dot h(t)+\frac{b^2}{\pi}\Phi_8\dot\alpha(t)\\+\frac{b^2}{2\pi^2}\Phi_2\Phi_\pi\dot\beta(t)+\frac{Bb}{\pi}\Phi_8(t)\\=\frac{Vb}{\pi^2}\Phi_1\Phi_8\beta(t)\end{aligned} \tag{A10}$$